Hindawi
International Journal of Aerospace Engineering
Volume 2022, Article ID 2410681, 15 pages
https://doi.org/10.1155/2022/2410681

Research Article

Hybrid Modeling Method of SDR Interstage Valve Based on Mechanism and Data-Driven

Hongfu Wang,[1] **Qinghua Zeng**,[1] **Xianhe Chen**,[2] **Zongyu Zhang**,[1] **and Weide Liu**[1]

[1]*College of Aeronautics and Astronautics, Sun Yat-sen University, Shenzhen, Guangdong Province 518107, China*
[2]*Company of Hongda Risheng Aerospace Power Technology, Changsha, Hunan Province 410005, China*

Correspondence should be addressed to Qinghua Zeng; zqinghua@sysu.edu.cn

Received 13 July 2022; Revised 16 September 2022; Accepted 12 October 2022; Published 25 October 2022

Academic Editor: Jun-Wei Li

Variable-throat adjustment is the most practical flow regulation method of solid ducted rocket ramjet (SDR). The high-fidelity mathematical model of the interstage valve is the basis for realizing high-precision gas flow and thrust regulation. In this paper, the complex effect of gas was divided into load and throat deformation effect. The load was mainly determined by the clearance, friction torque, and pneumatic torque that the valve was subjected to during operation. And the throat deformation was determined primarily by the deposition and ablation of the valve faced in the gas. Therefore, we could divide the valve model into three parts: the servo motor model, the load characteristic model, and the deformation model of the actual acting throat (referred to as the throat). Given, we have designed a cold-air experiment program, using cold air to equalize the valve load. Furthermore, we analyzed its mechanism of action and established the load model using the experimental data and neural network. Finally, the deformation mechanism of the throat was investigated, and simultaneously, the deformation model was shown based on the flight test data. Compared with the traditional interstage valve model, the model established in this paper is closer to the actual working conditions, which is helpful to carry out the more comprehensive and practical ground simulation. It has essential reference value for further realizing the precise regulation of gas flow.

1. Introduction

The SDR's gas flow regulation technology can realize the adjustable thrust of the aircraft, which is very important to recognize the wide envelope and large maneuvering flight of the aircraft [1]. Variable-throat regulation is the most practical way to regulate flow in SDR, that is, the flow is controlled by changing the throat area. Specifically, the oscillation of the valve causes a change in the throat area, resulting in different degrees of congestion and ultimately a change in the GG's (gas generator) pressure. The variation of pressure will modify the burning rate of the propellant, which in turn will cause the gas flow to the throat and the ram combustor (RC) to change, and the secondary combustion of the gas with the intake air will produce different thrusts [2, 3]. Although the SDR system is simple in structure, its operating boundary is narrow. For example, excessively high pressure in the RC may cause the air intake unstart, or even the ramjet to stall [4–6]. The gas flow is one of the main factors affecting the RC's pressure, so the high-precision response of the flow is a practical need in this research field.

However, to achieve high-precision flow response, it is necessary to establish a high-fidelity model of the valve, which is the guarantee for designing effective control laws. As shown in Figure 1, the traditional method only simplifies the valve as a servo motor for modeling [7, 8], ignoring the influence of load characteristics and throat deformation on flow regulation, which will undoubtedly bring more challenges to the accurate regulation of flow. The modeling approach proposed in this paper took the above factors into account for the first time, so the mathematical model of the valve was divided into three parts: the servo motor model, the load model, and the deformation model of the throat. Among them, the servo motor model was very common, so it was only covered in part B of the Supplementary Material (available here), while the other two parts were the research focus of this paper.

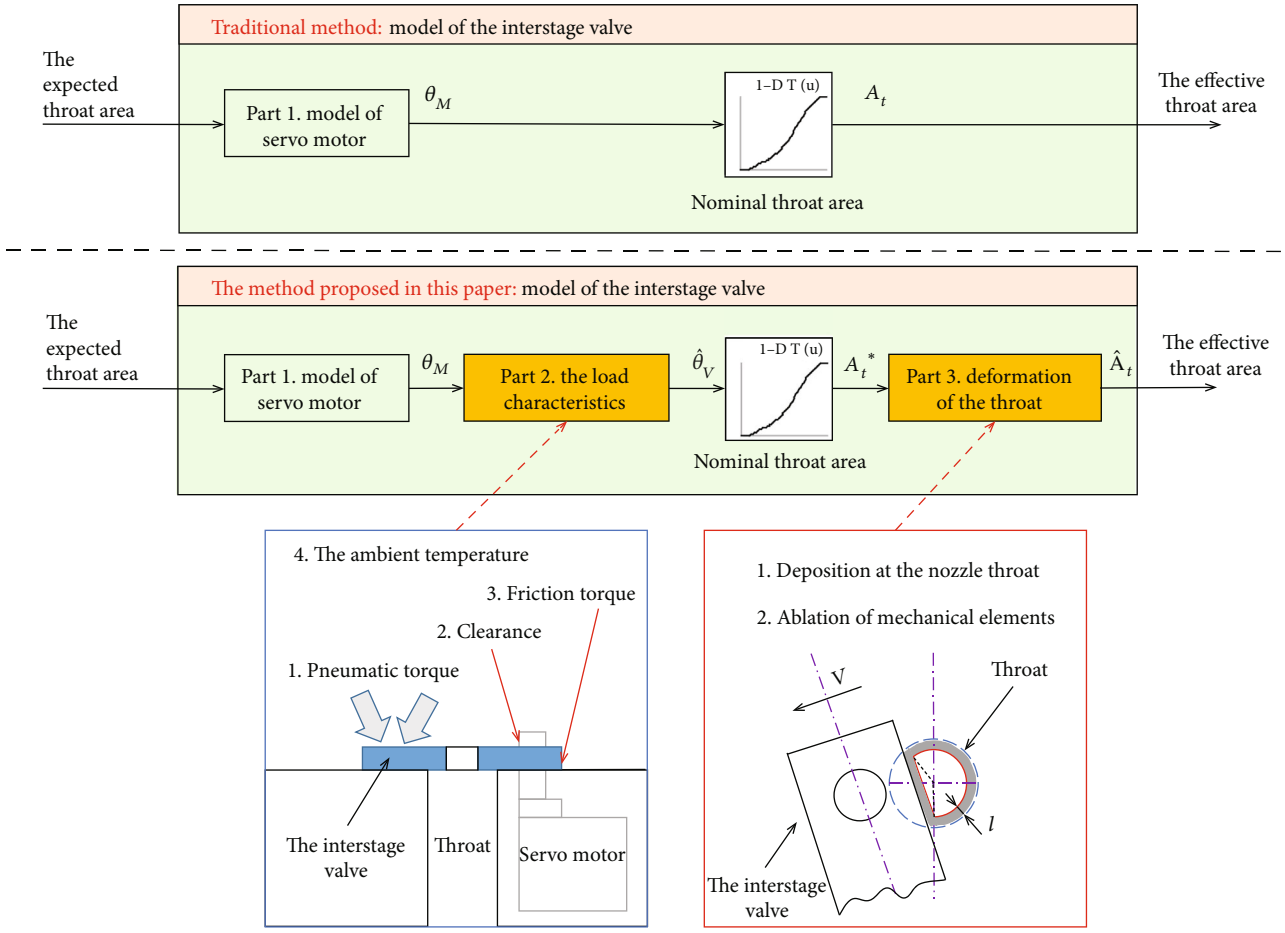

Figure 1: The composition and influencing factors of the valve mathematical model.

Mechanical clearance is one of the crucial factors affecting load characteristics; clearances in mechanical joints are unavoidable due to many uncertainties such as manufacturing tolerances, assemblage, wear, and material deformation [9]. The clearance between the mating parts leads to several complex dynamic phenomena such as surface contact, shock transmission, and the development of different regimes of friction and wear [10]. Therefore, a mechanical many-body system with clearance is a typical system with variable topology, and its model is more complex [11]. Xiang et al. used the Chebyshev polynomial method to analyze the dynamic response of a mechanical system with clearance joints. In this way, the approximate dynamic response range of the mechanism could be obtained, but the specific value of the clearance needs to be clarified [12]. For SDR systems, the load characteristics of the servo motor were divided into working load and system load, and the genetic algorithm was used for parameter identification [13]. However, it was not accurate to equate pneumatic load with the mechanical load.

The throat deformation is mainly caused by ablation and deposition, and the slag will be produced during the combustion process of the propellant. The production and deposition of slag are a very complex phenomenon, and it is difficult to predict accurately in SDR [14]. The production of slag in the gas generator (GG) will affect the established law of valve throat changes, thereby causing ramjet pressure disturbances and making the aircraft thrust unstable. Similarly, ablation of the throat and mechanical elements could also lead to performance degradation of SDR, affecting the thrust level of the ramjet and the specific impulse delivered [15]. Alanyalioglu pointed out that the real-time knowledge of the nozzle throat diameter plays an essential role in the analysis of the SDR after ignition, and the existing experimental methods for measuring the physical size of the nozzle throat diameter may not be suitable for every ramjet [16]. Li et al. proposed a nozzle throat ablation identification technology based on the ground test data of a ramjet, and the real-time change of the nozzle throat diameter during the operation was obtained [17]. The results showed that the change was small at the initial stage. With the increase in the working time, the throat diameter increased linearly, but this phenomenon is different from other types of ramjets.

Due to the high cost of the ground test, many researchers used cold-air experiments to evaluate the working conditions under gas in view of the complex mechanism in the working process. A closed-loop model reference adaptive controller was designed for the cold-air experiment equipment, but the device cannot truly reflect the gas changes in

the GG. For example, differences in gas parameters and free volume changes [18]. The valve displacement was controlled by changing the pressure in the valve head chamber, thereby changing the throat area. And a servo mechanism composed of a spring and guide rod was used to simulate the pressure in the GG (the force on the valve head had a linear relationship with the displacement) [19]. The device's purpose was to verify the control performance of the pneumatic servo system, and springs with different stiffnesses could be used to simulate the pressure in the GG. Liu achieved the purpose of adjusting the throat area by controlling the reciprocating motion of the cylinder [20]. The mathematical model of the GG was run in an industrial computer and outputted the pressure signal in real-time, which was equivalent to the force of the servo system and simulated the load of the actuator. The cold air was only used to drive the servo system. The test devices in Reference [21, 22] were designed to simulate the thrust of SDR, replacing the gas produced by propellant combustion with high-pressure air. Then, the relationship between the throat area and the thrust of the nozzle was analyzed. The experimental results showed that the measured pressure was consistent with the calculated value, but the measured thrust and the calculated one were inconsistent.

In summary, the interstage valve faces the tough influence of gas during the working process. More effective analysis methods are needed to evaluate the dynamic characteristics of the valve under complex working conditions. CFD can model the virtual flow field and perform fluid dynamics simulation; however, CFD has been an insurmountable problem in simulating turbulent flows with high accuracy. In view of the consistent properties exhibited by the SDR system in several experiments, we abandoned the use of CFD and proposed a hybrid modeling approach based on mechanistic and data-driven. Since the slide-interstage valve has the advantages of a simple structure and a large adjustment ratio [23]. This paper mainly studied the load characteristics and throat deformation characteristics of the slide-interstage valve during the operation. The main contributions are as follows:

(a) A cold-air experiment program was designed, and the complex influence of the clearance, friction torque, and pneumatic torque was simulated by the cold air. Furthermore, the action mechanism of the load on the valve was analyzed, and the load model was established through the cold-air experiment data.

(b) The deformation mechanism of the valve throat was analyzed, and its deformation model was established based on the flight test data. In addition, the influence of propellant parameters on the model was also investigated.

The rest of this paper was organized as follows. In Section 2, the operational characteristics of the valve were introduced, and the significance of analyzing the load characteristics was clarified again. In Section 3, the cold-air experiment program was designed, and the deformation mechanism of the valve was analyzed using the experiment data. Moreover, the load model of the valve was established by combining it with the neural network. The flight test data was used to model the throat deformation, and the propellant parameter perturbation was also considered in Section 4. And the conclusion and discussion were given in Section 5.

2. Working Characteristics of the Interstage Valve

During the working process of the SDR, the propellant is burned to generate gas, and the angle command of the valve is caused by the controller according to the gas flow required by the system so that the purpose of controlling the gas flow was achieved by adjusting the pressure in the GG. Since the valve will face high temperature and pressure inside the GG, it is usually difficult to directly measure the valve angle in this harsh environment, so the motor output angle is generally used to approximate the valve angle (only the motor angle is in the control loop). Although they are approximately equal under ideal conditions, the deviation between them cannot be ignored in this system. The swing range of the valve is 0-30 degrees, and the part of the throat was "blocked" by the valve swing. Thereby, the actual throat area is changed. The area enclosed by the solid red line represents the effective throat area (after this, referred to as the throat area) of the valve at different angles (as shown in Figure 2), which decreases with the decrease of the valve angle. A well-designed valve should have an approximately linear relationship between the throat area and the valve angle.

The basic principle of GG's mathematical modeling is the "law of conservation of mass", which means that the mass of gas generated by the combustion is equal to the mass of the gas inside the GG, adding the mass of discharge from the throat. In the paper, we follow the mathematical model of the GG established in Reference [24]; the process is not repeated, and the dynamic differential equation in the GG can be expressed in the form of Equation (1). (see part A in the Supplementary Material for scores analysis.)

$$\frac{dp_g}{dt} = \frac{R_g \cdot T_g}{V} \cdot \left(\rho_b \cdot A_b \cdot a \cdot {p_g}^n - \frac{p_g \cdot A_t}{C_r} \right), \tag{1}$$

where P_g is the gas pressure in GG, R_g is the gas constant, T_g is the gas temperature, and V represents the free volume, which means the volume between the propellant end face and the throat. ρ_b represents the propellant density, A_b represents the burning area of the propellant, a represents the propellant combustion rate coefficient, n represents the pressure index, and A_t represents the throat area. C_r represents the characteristic velocity of the gas.

According to Equation (1), the nonlinear model of the GG can be established, and the sensitivity coefficient (which indicates the increase in pressure for each 1-degree decrease when the valve is in different positions) of the system under different valve angles could be calculated. It can be seen from

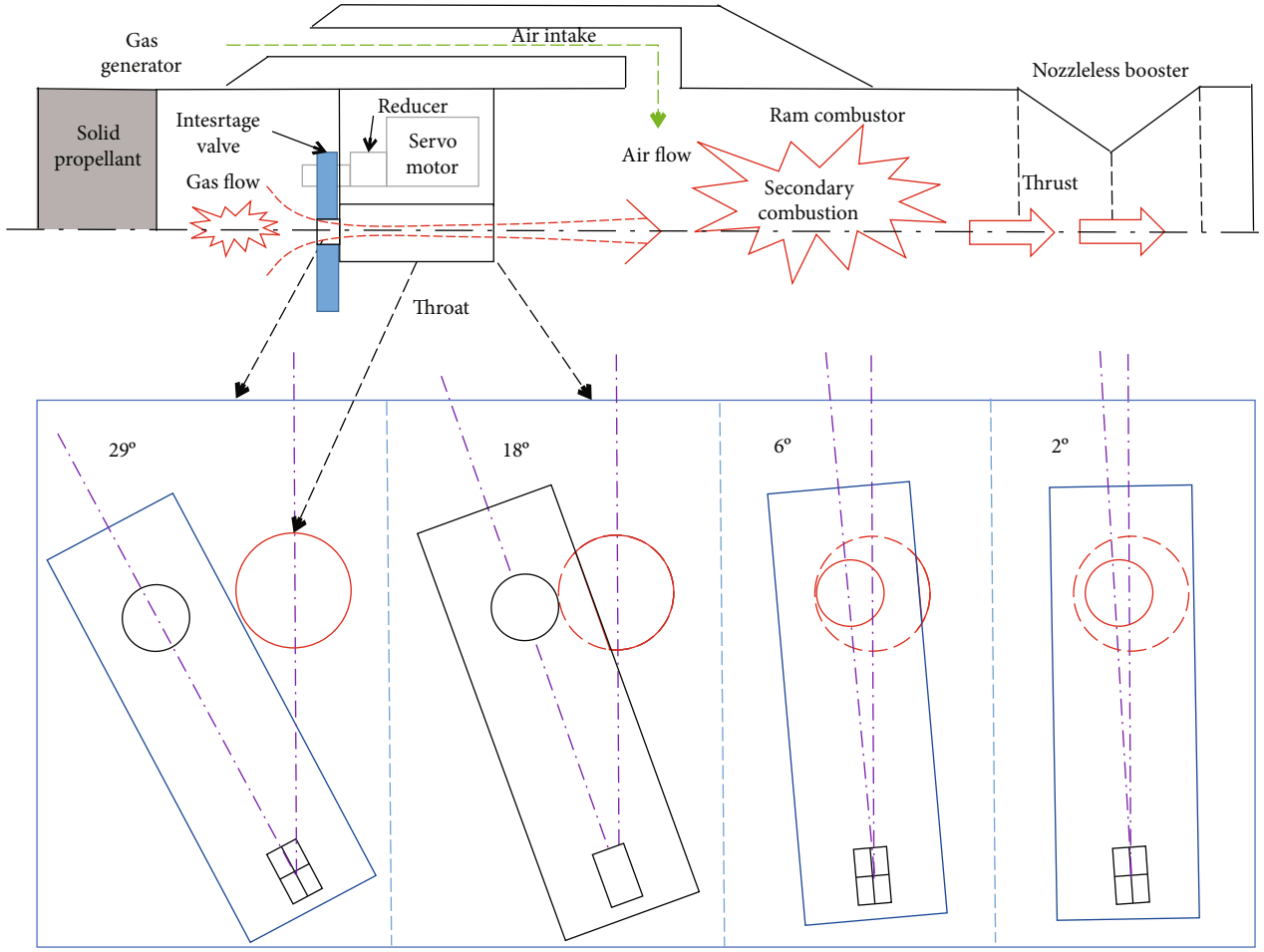

Figure 2: Schematic diagram of valve angle and throat area.

Figure 3 that when the valve angle is equal to 5 degrees, the most sensitivity coefficient is about 0.75 MPa/deg. When the valve angle is in the range of about 3 to 15 degrees, the sensitivity coefficient will be greater than 0.2 MPa/deg. The working conditions of the valve will affect the deviation between the valve angle and the command, which will affect the adjustment accuracy of the gas flow. Although the pressure control loop can correct the influence caused by valve deviation after a long enough time, the dynamic process of the pressure response needs to be strictly evaluated because the SDR has many constraints. In a word, for the gas flow regulation system that requires high control accuracy, it is significant to study the operational characteristics of the valve.

3. Load Characteristics of the Valve

Assuming that the valve is equally affected by clearance, pneumatic torque, and frictional torque at the same pressure. We can use the load under cold air to simulate ones under gas. The advantages of the cold-air experiment are the low cost, and the valve angle can be measured directly. The modeling principle of the valve was shown in Figure 4; firstly, based on the data measured in the cold-air experiments, the relationship between the valve angle and the motor angle under the load needs to be analyzed, and the load model of the valve should be established. Next, the estimated value of the valve angle ($\widehat{\theta}_V$) could be obtained through the flight test data and the load model of the valve. Then, the estimated throat area ($A_t{}^*$) could be obtained through the mapping relationship between the valve angle and the throat area. In addition, according to Equation (1), the relationship between the pressure and the throat area under dynamic equilibrium conditions could be obtained, as shown in Equation (2), so the real throat area (A_t) could be calculated. Its change process under the influence of ablation and deposition could be approximated by comparing $A_t{}^*$ and A_t.

$$A_t = \frac{K_T \bullet \eta \bullet \rho_b \cdot A_b \cdot a \cdot \left(1e^{-6}\right) \bullet C_r}{p_g{}^{(1-n)}}, \tag{2}$$

where K_T and η are the propellant temperature correction coefficient and the injection efficiency, respectively.

3.1. The Cold-Air Experiment Program. We specially developed a cold-air experiment equipment for this research (the equipment was only used to simulate the load), as shown in Figure 5. During the working process, the master

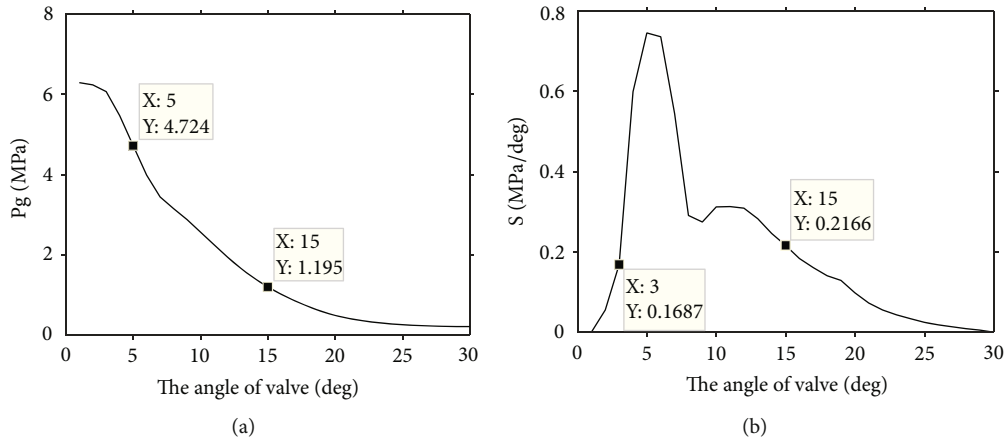

Figure 3: Relationship among pressure, sensitivity coefficient, and valve angle. (a) The valve angle and pressure. (b) The valve angle and sensitivity coefficient.

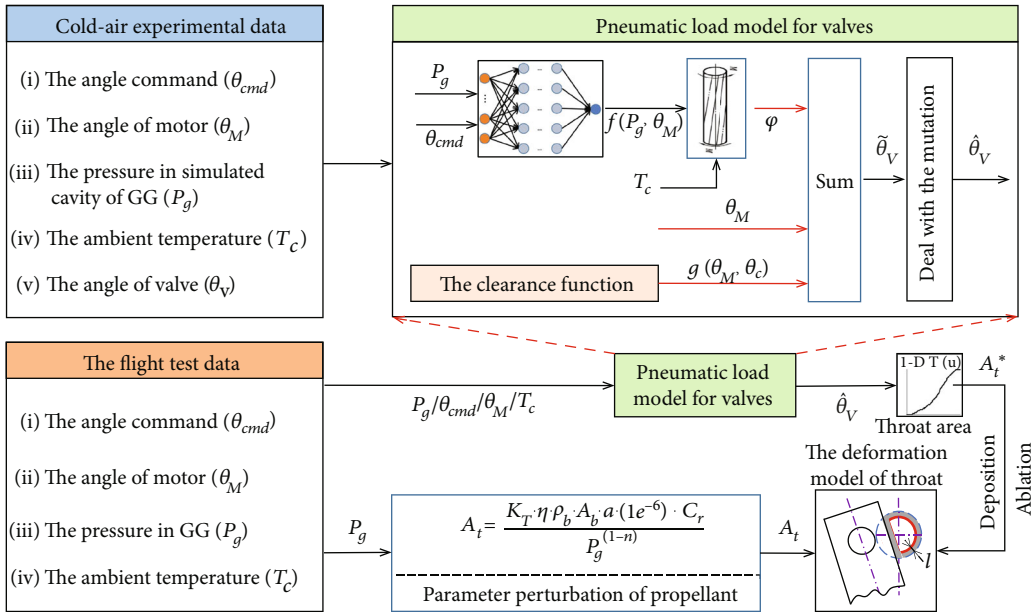

Figure 4: Fundamentals of building valve model.

console passed a certain amount of cold air into the simulated cavity of the GG (from now on, referred to as the GG) by controlling the air source. It monitored the pressure in real-time through the measurement data of the pressure sensor. Under this condition, for the servo motor control loop, the upper computer was used to send the planned command to the controller through the simulation and testing device, then the controller drove the motor and the valve to rotate. An angle sensor was embedded in the motor, which could feedback the motor angle to the controller. In addition, since the high temperature in the GG can be avoided under cold air conditions, we have installed an independent encoder on the valve body to measure its absolute angle of it. Since the valve was coaxial with the motor, under ideal conditions (It could be considered that the pressure in the GG was the standard atmospheric pressure), the valve angle was equal to the motor angle, but they began to differ after pressurization.

3.2. Cold-Air Experiments. In order to analyze the influence of the clearance on the load characteristics, the valve would be disassembled and installed several times in the experiments. It would be in different clearance states through corresponding technical means (refers to the clearance between the valve body and the transmission shaft). This instruction started from 30 degrees and decreased by 1 degree every 3 seconds until to zero, then rose by 1 degree every 3 seconds until 30 degrees. By injecting nitrogen gas into the GG, the maximum pressure in the GG was about 3 MPa, and the results were shown in Figure 6. It could be seen that the motor angle always maintained a good consistency with the command, and the maximum deviation was about 0.2

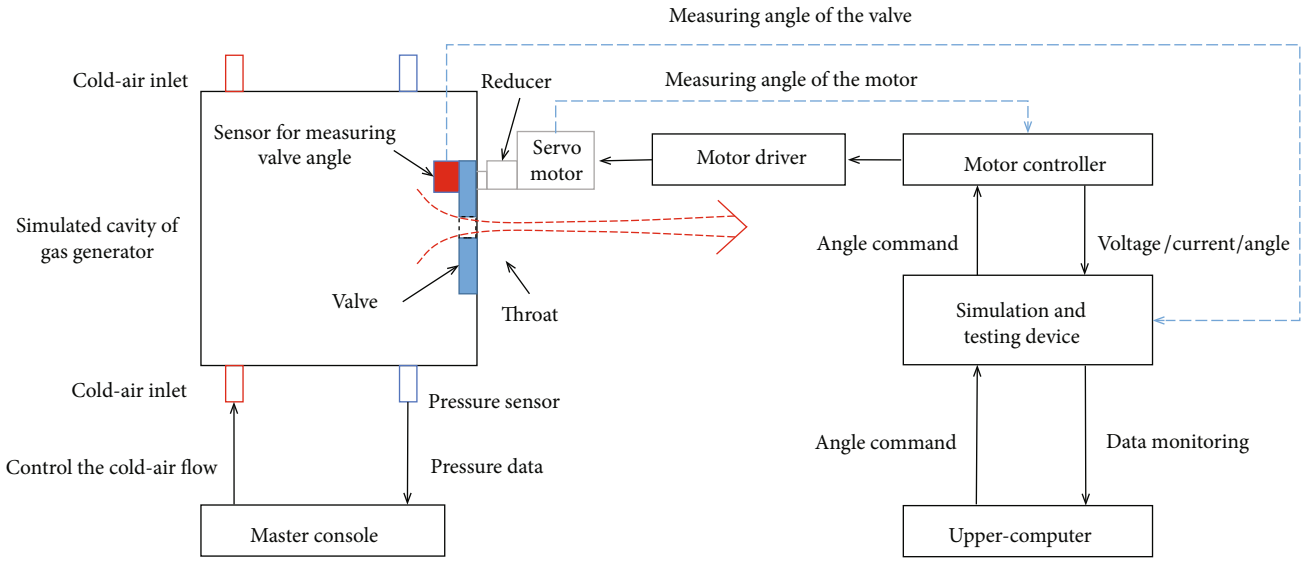

Figure 5: The working principle of the cold-air experiment device.

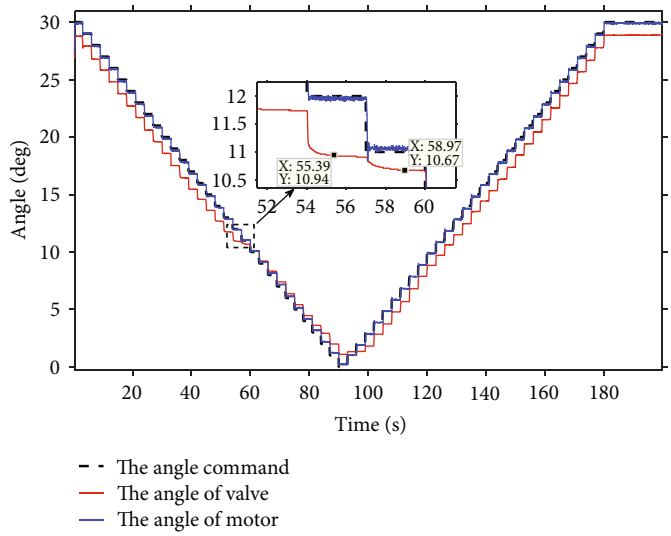

Figure 6: Valve angle response under large clearance conditions.

degrees. However, the consistency between the valve angle and the command was relatively poor. The most special one was around 11 degrees, and the motor typically swung about 1 degree following the command, but the valve only swung about 0.27 degree. In the area larger than 11 degrees, the valve angle was always smaller than the motor angle, while in the area less than 11 degrees, it was gradually larger than the motor angle. We could specify that the direction of the motor from 0 degrees to 30 degrees was "positive", and the opposite direction was "negative".

In order to fully demonstrate and study the load characteristics of the valve, we carried out experiments with different clearances and pressures under the same command. The error between the command and the valve angle was shown in Figure 7. It could be found that the mistake was maintained near 0 under atmospheric pressure, but it changed considerably after pressurization, and the higher the pressure, the greater the error. After the clearance was increased, the error between the command and the valve angle reached more than 1 degree. However, the load characteristics of the valve did not change, and the error changed from a positive value to a negative value within the specified area (about -12~2 degrees). Figure 8 showed the actual pressure in the GG under various conditions. It could be seen that under cold-air conditions, the clearance had little effect on the pressure, and the maximum deviation was only 0.186 MPa, which was different from the gas state. As shown in Figure 9, taking the valve angle under the working condition of "3 MPa/large clearance" as an example, the pressure deviation that could be caused in the open-loop state was the product of the valve angle deviation (Figure 7) and the sensitivity coefficient (Figure 3(b)). Figure 10 was a photo of the

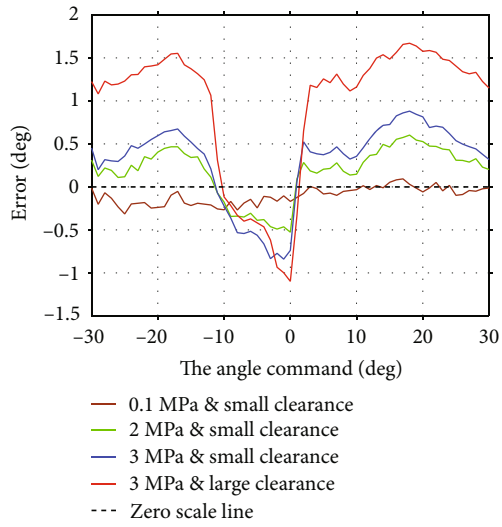

Figure 7: The error between valve angle and command.

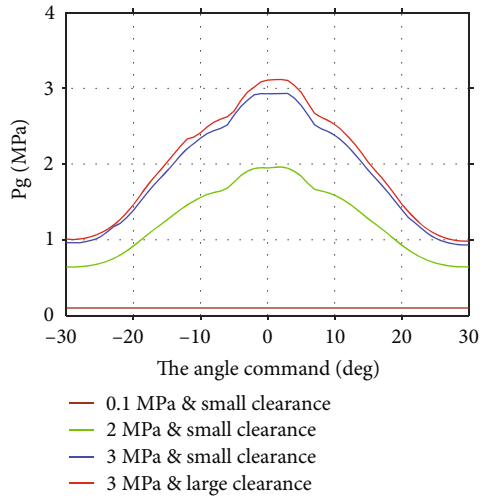

Figure 8: The actual pressure in the GG.

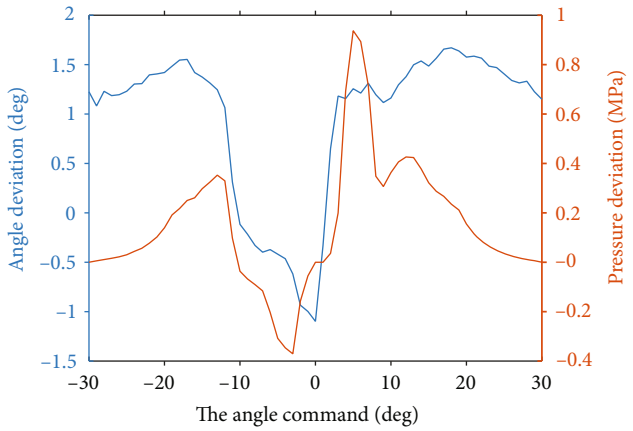

Figure 9: Pressure deviation under the condition of "3 MPa/large clearance".

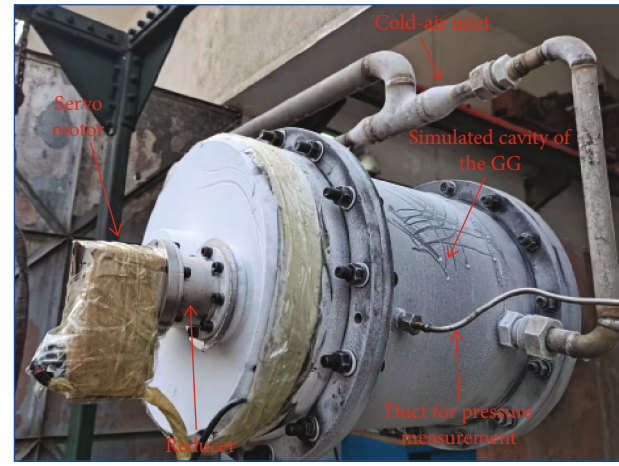

Figure 10: Cold-air experiment site.

cold-air experiment site; during the experiment, the water vapor in the air condensed into frost and adhered to the outer wall of the GG.

Immediately afterward, we carried out the second experiment. At this time, after the instruction was followed for about 1 second, we began to inject nitrogen to increase the internal pressure of the GG. In this way, we could see the relative change of the valve angle and the motor angle before and after the pressurization. As shown in Figure 11, it could be found that after the pressurization, there was a deviation of about 0.68 degree between the valve angle and the motor angle. The deviation value also showed a trend of "first increase, then decrease, first positive, then negative". In this experiment, the angle error between the motor and the valve changed from positive to negative at around 8 degrees. At this position (dynamic equilibrium state), the resultant force of the valve could be regarded as 0. We called the valve angle at this time the "balance angle". Then comparing Figure 6, it could be seen that the "balance angle" of the valve was not fixed, and it was related to the assembly process of the valve. The pressurization ended after about 48.5 seconds, and the deviation returned to a small value at this time, indicating that the valve deforms elastically instead of plastically under pneumatic load conditions.

Then, the two commands were triangular waves with variable frequency, the command cycles were 2 seconds and 12 seconds, respectively, and the slopes were 3 degrees/second and 0.5 degrees/second, respectively. Figure 12(a) reflected the valve response between 18 degrees and 15 degrees (in the area above the "balance angle"), the valve angle was always smaller than the motor angle, the pressurization ends in about 32 seconds, and then the deviation between the two curves gradually returned to a smaller value. However, Figure 12(b) reflected the valve response between 8 degrees and 5 degrees (in the area below the "balance angle") when the direction of the motor was changed, the angle deviation changed from negative to positive, which was an uncertainty error for flow regulation, and this load characteristic had a significant influence on gas flow regulation.

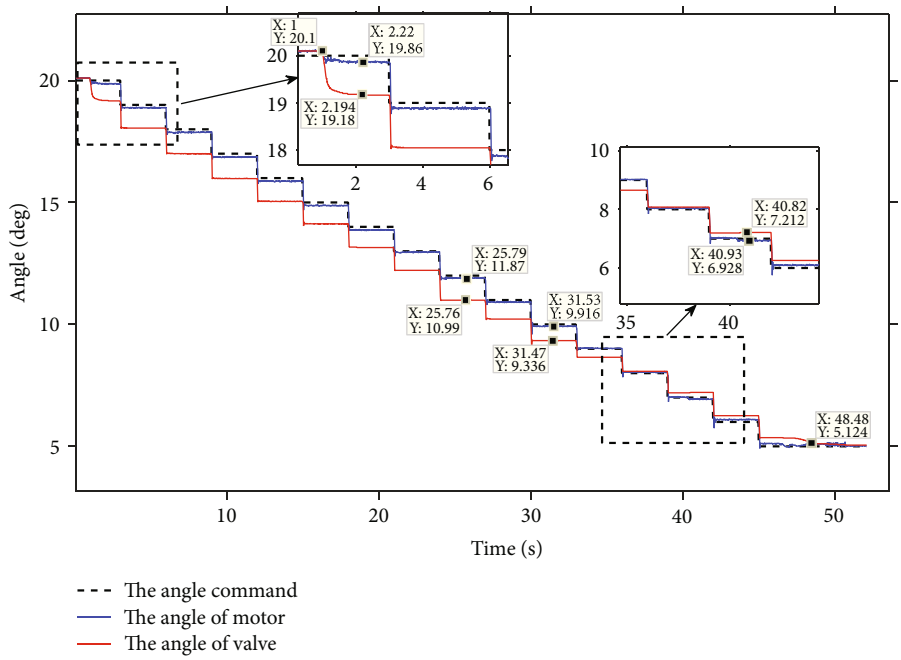

Figure 11: Valve angle response under large clearance conditions (second experiment).

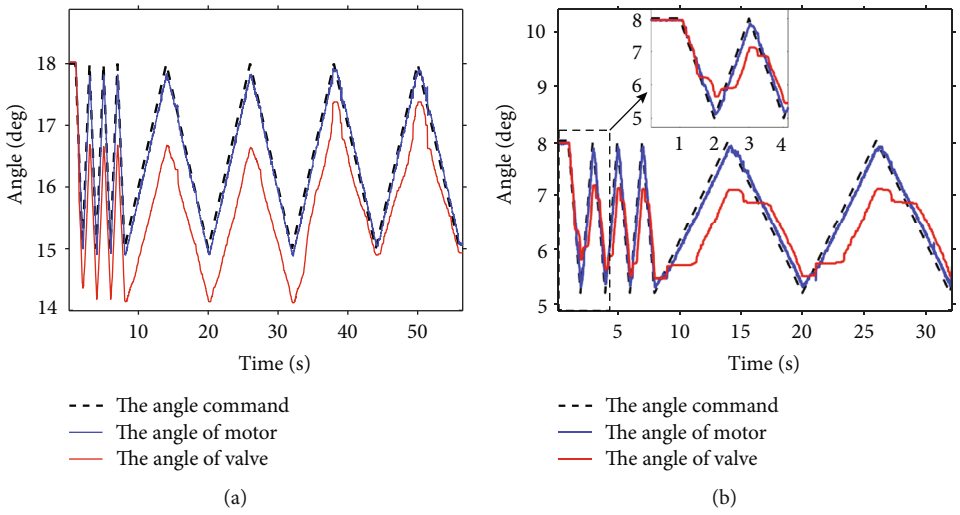

Figure 12: Valve response under a triangular wave (second experiment). (a) Reaction between 15–18 degrees. (b) Reaction between 5–8 degrees.

3.3. The Load Action Mechanism and the Load Model of the Valve. As mentioned above, the valve deformed elastically under pneumatic load. As shown in Figure 13, the encoder was installed on the valve connecting the shaft, and its measurement value could reflect the torsional deformation of the shaft. The torsional deformation of the shaft was calculated as shown in Equation (3), Equation (4) was the calculation method of shear modulus, and for the solid circular section, Equation (5) holds.

$$\varphi = \frac{T \bullet L}{G \bullet I_P}, \tag{3}$$

$$G = \frac{E}{2 \bullet (1 + \mu)}, \tag{4}$$

$$I_P = \frac{\pi \bullet D^4}{32}, \tag{5}$$

where the G is the shear modulus, the I_P is the polar moment of inertia (the $G \bullet I_P$ is often referred to as torsional stiffness), the D is the diameter of the circular shaft section, the T is the torque received by the shaft, and the L is the length of the shaft. The E is the elastic modulus, and the μ is Poisson's ratio.

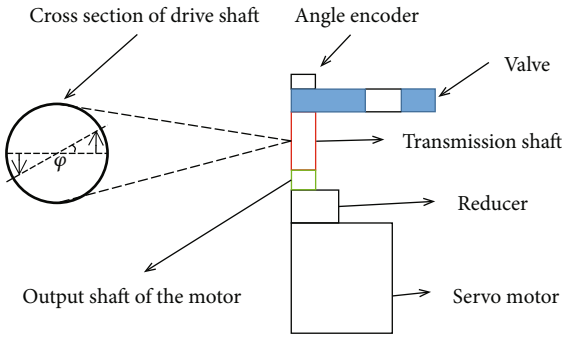

Figure 13: Deformation of the valve connecting shaft.

Based on the measurement results, the deformation of the shaft could also be expressed in the form of Equation (6), which means that both deformation and clearance factors are implicit in the measurement (θ_V). The torsional deformation of the valve is mainly caused by the lateral force, so the torque on the valve could be expressed by Equation (7), which means that the lateral force on the valve is mainly affected by the pressure and the valve angle.

$$\varphi = [\theta_M - \theta_V - g(\theta_c, \theta_M)] * \frac{\pi}{180}, \tag{6}$$

Among them, θ_V is the valve angle (equivalent to θ in Equation (2)), θ_M is the motor angle, θ_c is an unknown but determined clearance value, and $g(\theta_c, \theta_M)$ is defined as the clearance function.

$$T = F_c \bullet L_V = f(P_g, \theta_M) \bullet L_V, \tag{7}$$

where F_c is the total lateral force on the valve, L_V is the length of the slide-interstage valve, and $f(P_g, \theta_M)$ is defined as the pressure function.

In the small clearance state, $g(\theta_c, \theta_M) \approx 0$, if θ_V and θ_M are known, $f(P_g, \theta_M)$ at each position in the current state can be obtained. We believe that $f(P_g, \theta_M)$ under the same pressure is approximately the same, so the $g(\theta_c, \theta_M)$ of the same pressure but large clearance state can be calculated according to Equation (8). Figure 14 reflected the value of $g(\theta_c, \theta_M)$ at different angles.

$$g(\theta_c, \theta_M) = (\theta_{M2} - \theta_{V2}) - (\theta_{M1} - \theta_{V1}) \approx \theta_{V1} - \theta_{V2}, \tag{8}$$

Among them, subscript 2 represents the measurement value in the state of large clearance, and subscript 1 represents the measurement value in the form of small clearance. Since the size of the clearance does not affect the output angle of the motor, $\theta_{M2} \approx \theta_{M1}$.

In different states, the lateral force on the valve was shown in Figure 15. Due to the complex force mechanism of the valve in the pressurized state, this paper chose to use a neural network to approximate $f(P_g, \theta_M)$ to obtain the value under different pressures. The network input was pressure and angle command (including direction information), and the output was the lateral force on the valve, namely f

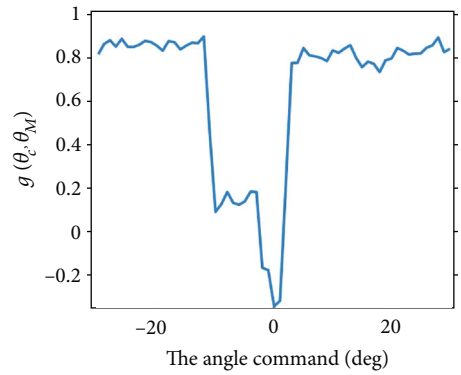

Figure 14: The value of $g(\theta_c, \theta_M)$ at different angles.

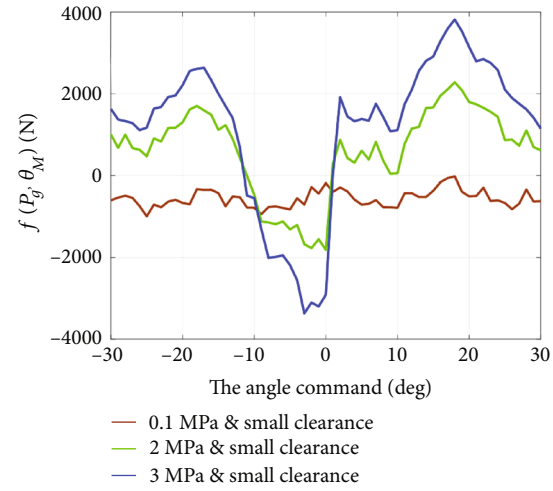

Figure 15: Lateral force on the valve.

(P_g, θ_M). The Bayesian regularization algorithm provided in MATLAB was used for training, and different hidden layers were selected for additional training effects. Take the experimental condition with the maximum value of 2 MPa as an example, if Equation (9) was used to evaluate the similarity of the two sets of data, Figure 16(a) showed that the fitting effect was the best when the number of hidden layers was 35, and the F value was 59.5. Figure 16(b) was the intuitive result of its fitting effect.

$$F = \int_0^t |M_1(t) - M_2(t)| \bullet dt, \tag{9}$$

where M_1 and M_2 represent different data, respectively, and t represents the time.

Finally, we could obtain the theoretical value of the valve angle according to the experiment's results, as shown in Equation (10), where the elastic modulus E is related to the temperature, so it is represented by $E(T_c)$. (In the experiment, the θ_M was the measured data, while in the simulation, it was obtained from the mathematical model of the motor, see part B in the Supplementary Material for the motor's

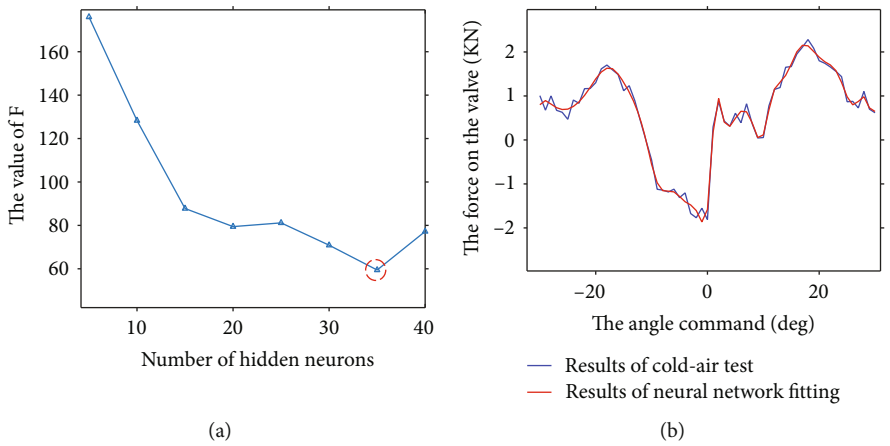

FIGURE 16: Fitting of lateral force by a neural network. (a) The relationship between F value and hidden layer. (b) Fitting effect of 35 hidden layers.

mathematical model.)

$$\widetilde{\theta}_V = \theta_M - \frac{2 \bullet f\left(P_g, \theta_M\right) \bullet L_V \bullet L \bullet (1+\mu)}{E(T_c) \bullet I_P} * \frac{180}{\pi} - g(\theta_c, \theta_M), \tag{10}$$

where $\widetilde{\theta}_V$ is the theoretical value of the valve angle, and the T_c is the temperature of the shaft.

However, calculating the hypothetical value of the valve according to Equation (10) would face a problem, that, when the valve changes its motion direction in the area below the "balance angle", its theoretical value will change abruptly due to the change in the action direction of the force, but this does not satisfy the laws of physics (refer to Figure 12(b)). Therefore, this paper used Equation (11) to Equation (13) to deal with this mutation. A constant value was maintained for some time when the valve changed the direction of movement, which was equivalent to the effect of the adaptive width "dead zone".

$$\begin{cases} I_A(t) = \widetilde{\theta}_V(t) \\ I_A(t) = I_B(t-1) \end{cases}, \quad \begin{matrix} \widetilde{\theta}_V(t) > I_B(t-1) \& \dfrac{d\theta_{\text{cmd}}}{dt} > 0, \\ \widetilde{\theta}_V(t) \le I_B(t-1) \& \dfrac{d\theta_{\text{cmd}}}{dt} > 0, \end{matrix} \tag{11}$$

$$\begin{cases} I_B(t) = I_A(t-1) \\ I_B(t) = \widetilde{\theta}_V(t) \end{cases}, \quad \begin{matrix} \widetilde{\theta}_V(t) > I_A(t-1) \& \dfrac{d\theta_{\text{cmd}}}{dt} \le 0, \\ \widetilde{\theta}_V(t) \le I_A(t-1) \& \dfrac{d\theta_{\text{cmd}}}{dt} \le 0, \end{matrix} \tag{12}$$

$$\begin{cases} \widehat{\theta}_V(t) = I_A(t) \\ \widehat{\theta}_V(t) = I_B(t) \end{cases}, \quad \begin{matrix} \dfrac{d\theta_{\text{cmd}}}{dt} > 0, \\ \dfrac{d\theta_{\text{cmd}}}{dt} \le 0, \end{matrix} \tag{13}$$

where $\widetilde{\theta}_V$ represents the estimated value of the valve angle, and θ_{cmd} is the angle command.

3.4. Validation of the Load Model. The load model was established based on the data from the first cold-air experiment. The prediction of the second experiment results using the load model was reflected in Figure 17, which reflected the comparison between the estimated valve angle and the actual measured value; Figure 17(a) showed that the valve changed the direction of movement in the area bigger than the "balance angle", and Figure 17(b) showed that the valve altered the direction of motion in the space smaller than the "balance angle". Although the "balance angle" in the two experiments was inconsistent, they were relatively close and had the same characteristics. The results showed that the method could accurately predict the dynamic response of the valve under pneumatic load.

The elastic modulus of almost all metals and alloys is temperature dependent, normally, the elastic modulus of the metal decreases with the increase of temperature [25, 26], which means that under the same external force, the higher the temperature, the greater the deformation of the metal. Especially for valves that work under high temperature and pressure conditions, the temperature factor cannot be ignored. For the connecting shaft in this paper, its elastic modulus is about 200 GPa at 25∘C, and its elastic modulus is about 150 GPa at 900∘C. Therefore, the relationship between the elastic modulus and temperature was approximately expressed in Equation (14). According to the temperature rise history of a point in the conductor described in Reference [27], we used the first-order inertia link to simulate the temperature rise process of the connecting shaft according to its final temperature (about 500∘C) and the action time. The time constant was set to 50, as shown in Equation (15), which will be helpful in modeling throat deformation in the next chapter.

$$E(T_c) \approx -0.057 \bullet T_c + 201.43, \tag{14}$$

$$T_c(s) = \frac{1}{50 \bullet s + 1}. \tag{15}$$

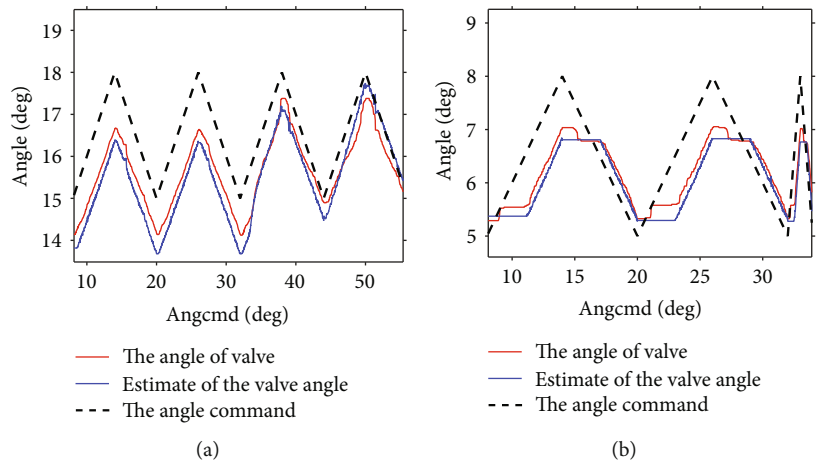

Figure 17: Valve estimates vs. actual measurements under cold-air experiment. (a) The response between 15–18 degrees. (b) The response between 5–8 degrees.

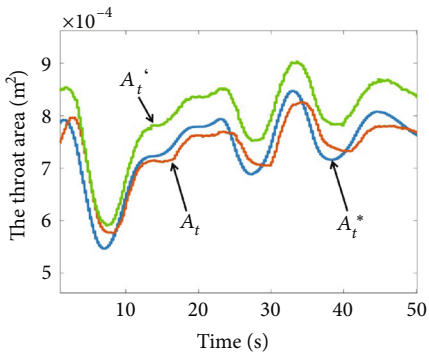

Figure 18: Estimation of throat area based on the load model.

As shown in Figure 18, taking a flight test participated by our research group as an example, on the one hand, the change of the actual throat area could be estimated according to the real-time measured pressure in the GG, which was represented by A_t. On the other hand, according to the load model, the change of the throat area under pneumatic load could be estimated, which was represented by A_t^*. To illustrate the effectiveness of the valve load model, we added a control group, which evaluated the throat area according to the motor angle measured in the test, denoted by A_t' (traditional method, equivalent to no deformation of the connecting shaft). It could be seen that A_t^* was closer to A_t than A_t' (F values are 0.001145 and 0.003128, respectively); this could also illustrate the validity of the load model.

4. Throat Deformation Model

4.1. The Mechanism Analysis and Modeling Process. As mentioned above, the change of throat area during flight could be roughly estimated by the measurement pressure and combined with the load model of the valve, and the transformation of the throat area under the influence of ablation and deposition could be deduced. During the cruise segment of the aircraft, to save fuel and ensure the voyage, the swing range of the valve is usually tiny. The valve is usually opened at a large degree to maintain a small flow (in this flight test, the valve angle was basically kept above 18 degrees when the cruise section). Since the cruise segment lasts long, it is the main period for throat ablation and deposition. Therefore, we focused on analyzing the deformation of the throat area during the cruise segment (as shown in Figure 19),and established its model. After deposition, the effective throat area can be approximately calculated according to Equation (16) (if ablation occurs, l is a negative value).

$$A_t = \frac{360 - \gamma\left(\widehat{\theta}_V\right)}{360} \bullet \pi \bullet [R - l(t)]^2 + 2 \bullet [R - l(t)] \bullet \sin\frac{\gamma\left(\widehat{\theta}_V\right)}{2} \bullet \cos\frac{\gamma\left(\widehat{\theta}_V\right)}{2}, \tag{16}$$

where R is the throat radius, and l is the variation of the throat radius

In the initial state, deposition or ablation does not occur, that, when $l(t) = 0$, according to Equation (16), the approximate value of γ in the range of 18~27 degrees can be obtained based on the least square method (in the initial state, A_t was known). As shown in Figure 20, the relational expression of γ can be obtained by polynomial fitting, and the result was shown in Equation (17).

$$\widehat{\gamma}\left(\widehat{\theta}_V\right) = -15.17 \bullet \widehat{\theta}_V + 419.4, \tag{17}$$

When $l(t) \neq 0$, A_t can be obtained from Equation (2), and into Equation (16), and the expression of l can be found by bringing A_t into Equation (16), Equation (18) is the analytical expression of $l(t)$ when A_t was known. Since our purpose is to establish an estimation model of A_t, we also need to fit $l(t)$ here. Assuming that l is only related to t when the valve swing range is not extensive, we could use a cubic polynomial to fit $l(t)$, and the result was shown in Figure 21. The

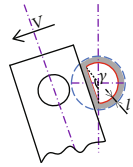

Figure 19: Deformation in throat area when ablation or deposition occurs.

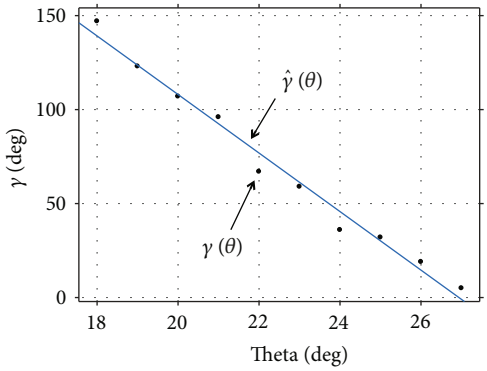

Figure 20: Fit to $\gamma(\theta.)$.

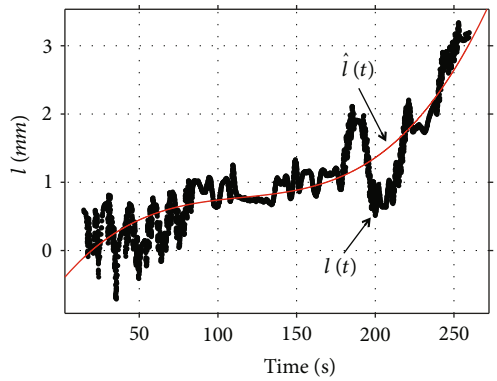

Figure 21: Fit to $l(t)$.

fitting expression is Equation (19).

$$l(t) = R - \frac{\sqrt{B_d{}^2 + 4 \bullet A_d \bullet A_t{}^*(t)} - B_d}{2 \bullet A_d}, \tag{18}$$

where $A_d = 360 - \gamma(\theta)/360 \bullet \pi$, and $B_d = 2 \bullet \sin \gamma(\theta)/2 \bullet \cos \gamma(\theta)/2$.

$$\widehat{l}(t) = a_1 \bullet t^3 + a_2 \bullet t^2 + a_3 \bullet t + a_4, \tag{19}$$

where $a_1 = 6.354 \bullet 10^{-7}$, $a_2 = -2.197 \bullet 10^{-4}$, $a_3 = 2.766 \bullet 10^{-2}$, and $a_4 = -0.4642$.

For the convenience of calculation, we can perform Taylor expansion on the trigonometric terms in Equation (16), and only keep the first three terms. Finally, we could obtain the estimated value of the throat area as shown in Equation (20), where $\widehat{\theta}_V$ could be calculated by Equation (10)–(13).

$$\widehat{A_t} = \frac{360 - \widehat{\gamma}\left(\widehat{\theta}_V\right)}{360} \bullet \pi \bullet \left[R - \widehat{l}(t)\right]^2 + 2 \bullet \left[R - \widehat{l}(t)\right] \bullet M_S \bullet M_C, \tag{20}$$

where

$$\begin{cases} \sin \dfrac{\gamma\left(\widehat{\theta}_V\right)}{2} \approx M_S = x_S - \dfrac{x_S{}^3}{3!} + \dfrac{x_S{}^5}{5!}, \\ \cos \dfrac{\gamma\left(\widehat{\theta}_V\right)}{2} \approx M_C = 1 - \dfrac{x_S{}^2}{2!} + \dfrac{x_S{}^4}{4!}, \\ x_S = \dfrac{\gamma\left(\widehat{\theta}_V\right)}{2} \bullet \dfrac{\pi}{360}. \end{cases} \tag{21}$$

It could be seen from Figure 22 that $\widehat{A_t}$ was closest to A_t, while $A_t{}^*$ was the second closest, and $A_t{}'$ was the most different from A_t, which showed the validity of the throat deformation model developed in this section (F values were given centrally in Table 1). In addition, since $l(t)$ was always greater than 0 in the cruising segment (enter the cruise section at about 30 seconds), this indicated that the deposition was the main effect during this period. In summary, if the valve satisfies the two conditions that the angle is greater than 18 degrees, and the swing range is small, the valve model established in this paper is very effective. As shown in Figure 23, we could use the established model (the load model and the throat deformation model) to make an accurate prediction of the throat area in a specific ground test (the swing range of the valve was about 19~23 degrees).

4.2. Influence of Propellant Parameter Perturbation on Throat Identification. The above analysis was done without considering the perturbation of propellant parameters. However, solid propellants have many components and complex reactions. They do not all meet the "ideal conditions" during the working process, and many parameters will be perturbed. For example, it was pointed out in Reference [28] that due to the explosion of the ignition charge, the end face of the propellant grain has pits, and then burns continuously in the form of pits, which indicates that the actual burning area may be larger than the designed burning area. In addition, it was also pointed out that because the manufacturers mainly used noninsulated gas generators in the test process for the C_r, the heat loss was relatively significant; Hence, the nominal value of the measured C_r was lower than the actual value. When the pressure index (n) is constant, the logarithm of the burning rate (r) and the logarithm of the pressure (P_g) are approximately linear [29, 30]. However, the n is not an absolute constant in the existing system. Especially with a higher-pressure range in GG, the n is more significantly affected by P_g. From Equation (2), it could be seen that the influence of other parameters on the evaluation of A_t is equivalent except for the n, and they are all

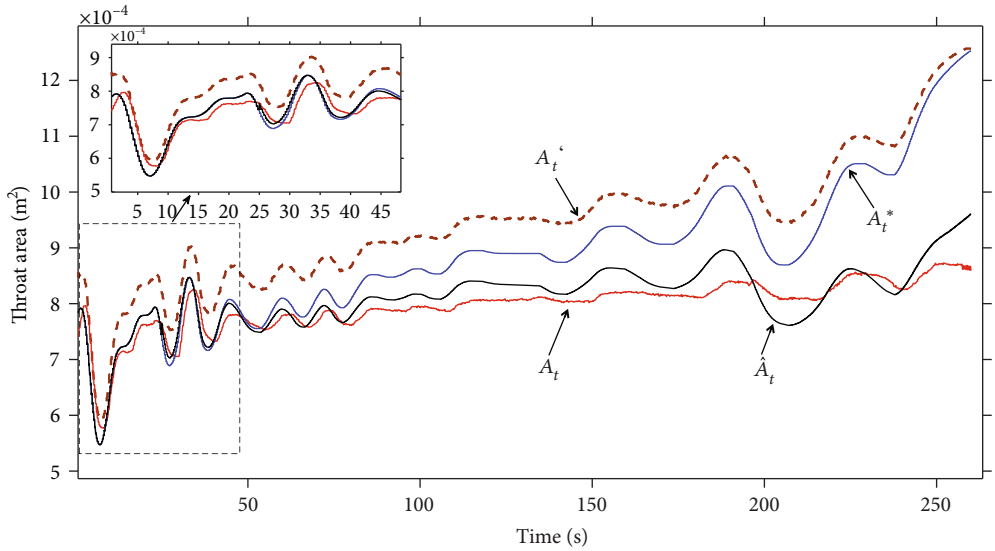

Figure 22: Estimation of throat area under various conditions.

Table 1: The F values in each case.

Period (s)	Object of comparison	F values
0 ~ 50	A_t^* & A_t	0.0011
0 ~ 50	A_t' & A_t	0.0031
0 ~260	A_t^* & A_t	0.0254
0 ~260	A_t' & A_t	0.0397
0 ~260	$\widehat{A_t}$ & A_t	0.0066
0 ~260	A_t^* & $A_t$under C_r perturbation	0.0120
0 ~260	A_t^* & $A_t$under n perturbation	0.0210

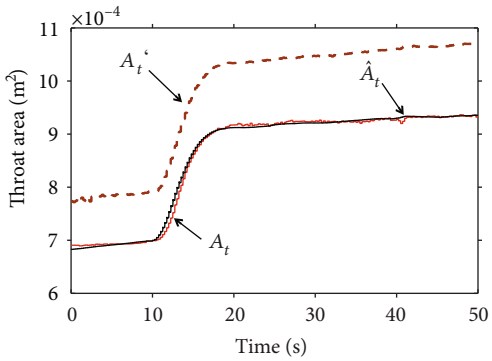

Figure 23: Prediction of throat area in ground tests using the throat deformation model.

proportional to A_t. Therefore, we would focus on analyzing the influence of C_r and n on the accuracy of A_t's identification.

For a positive n propellant, $n \in (0, 1)$, so according to Equation (2), when $P_g > 1MPa$, the smaller the n, the smaller the A_t. When $P_g < 1MPa$, the smaller the n, the larger the A_t. Assuming the C_r and n were perturbed according to Equation (22) and Equation (23), respectively, relative

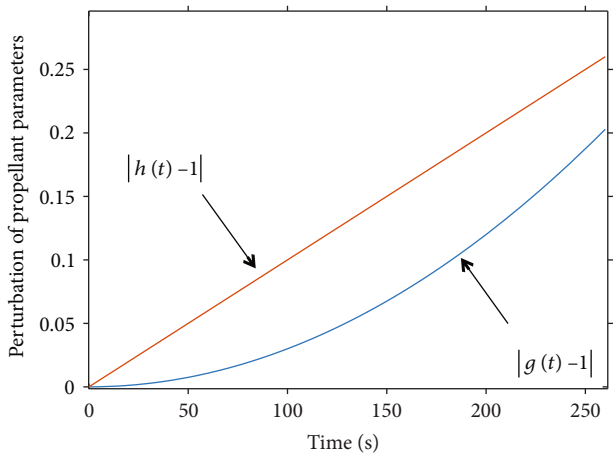

Figure 24: Perturbations of C_r and n.

to the nominal value, as shown in Figure 24, the maximum perturbation of the C_r was about +20%, and the maximum perturbation of the n was about -25%. The simulation results were shown in Figure 25. Compared with n, the C_r could cause a wider range of changes in the identification. Finally, the F values describing the closeness of A_t and A_t^* in each case were counted in Table 1.

$$\begin{cases} C_r^* = g(t) \bullet C_r, \\ \ddot{g(t)} = k_1, \\ g(0) = 1, \dot{g(0)} = 0, \end{cases} \tag{22}$$

$$\begin{cases} n^* = h(t) \bullet n, \\ \dot{h(t)} = k_2, \\ h(0) = 1, \end{cases} \tag{23}$$

where $k_1 = 6 \bullet (1e^{-6})$, $k_2 = -(1e^{-3})$.

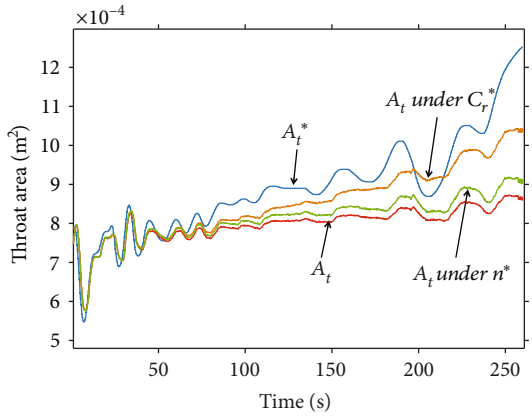

Figure 25: Influence of propellant parameter perturbation on throat identification.

5. Conclusion

A high-fidelity valve model is essential to achieve high-precision regulation of gas flow. In this paper, the load and deformation problems were faced squarely for the first time, and a complete valve model was established by combining the experimental data and analyzing its action mechanism. The following conclusions were finally obtained:

(a) In this paper, a cold-air experiment scheme was designed, in which the cold air was used to simulate the loading effect of gas on the valve, and further the neural network was used to fit the force of the valve during the operation. Based on this, the deformation angle of the connecting shaft could be obtained, and the load model of the valve was finally established. At the same time, we also illustrated the accuracy of the load model using experimental data.

(b) Based on the flight test data, we used a polynomial fitting method to establish the relationship between the deposition thickness and time, based on which the deformation of the throat area at the same angle could be obtained, and finally the deformation model could be established. Through the experimental data, the accuracy of the model was illustrated. But it was influenced by the propellant parameters, which was limitation of the model.

(c) In the traditional method, the valve angle was simply approximated by the output angle of the servo motor. However, for the first time, we have established the load model and the throat deformation model, which, together with the servo motor model, constitute a complete valve model, which will help to carry out more effective ground simulation.

Nomenclature

θ_c: Mechanical clearance
θ_V: The angle of the valve
θ_M: The angle of the motor
θ_{cmd}: The angle command
$\widehat{\theta}_V$: The predicted value of the valve angle
$\widetilde{\theta}_V$: The theoretical value of the valve angle
P_g: The gas pressure in GG
R_g: The gas constant
T_g: The gas temperature
V: The free volume
ρ_b: The propellant density
A_b: Burning area of the propellant
a: The propellant combustion rate coefficient
n: The pressure index
C_r: The characteristic velocity of the gas
A_t: The actual throat area
A_t^*: The throat area under load conditions
F: Fitting accuracy
C_r^*: The characteristic velocity in Disturbed Conditions
n^*: The pressure index in disturbed conditions
K_T: The propellant temperature correction factor
η: Injection efficiency correction factor
φ: Deformation angle of the connecting shaft
G: Shear modulus of the connecting shaft
I_p: Polar moment of inertia
D: Diameter of the connecting shaft
T: Torque on the connecting shaft
L: Length of the connecting shaft
E: Elastic modulus of the connecting shaft
μ: Poisson's ratio
L_V: Length of the slide valve
F_c: The resultant force in the lateral plane
T_c: The temperature of the connecting shaft
A_t': The throat area under ideal conditions.

Data Availability

Data used to support the findings of this study are available from the corresponding authors upon request.

Conflicts of Interest

The authors declare that there is no conflict of interest regarding the publication of this paper.

Acknowledgments

I would like to show my deepest gratitude to my supervisor, Dr. Zeng Qinghua, a respectable and resourceful scholar, who has provided me with valuable guidance in every stage of the writing of this thesis. This research is financially supported by the National Natural Science Foundation of China (Grant No. 61174120).

Supplementary Materials

The detailed derivation process of Equation (1) was supplemented in part A, and the mathematical model of the servo motor and the calculation method of θ_M were provided in part B. *(Supplementary Materials)*

References

[1] Z. Xia, B. Chen, L. Huang, D. Wang, and L. Ma, "Research progresses in solid rocket-ramjet engine," *Aerospace Shanghai*, vol. 36, no. 6, pp. 11–18, 2019.

[2] H. Wang, Q. Zeng, A. Wang, and Z. Zhang, "Application of gap metric to LADRC design in multilinear model of SDR," *International Journal of Aerospace Engineering*, vol. 2022, Article ID 2669954, 13 pages, 2022.

[3] A. Wang, Q. H. Zeng, L. K. Ma, and H. Wang, "Adaptive backlash compensation method based on touch state observation for a solid cucted rocket," *International Journal of Aerospace Engineering*, vol. 2020, Article ID 6698158, 12 pages, 2020.

[4] J. Chang, D. Yu, W. Bao, and Y. Fan, "Operation pattern classification of hypersonic inlets," *Acta Astronautica*, vol. 65, no. 3-4, pp. 457–466, 2009.

[5] D. Yu, J. Chang, W. Bao, and Z. Xie, "Optimal classification criterions of hypersonic inlet start/unstart," *Journal of Propulsion and Power*, vol. 23, no. 2, pp. 310–316, 2007.

[6] J. Chang, D. Yu, W. Bao, Z. Xie, and Y. Fan, "A CFD assessment of classifications for hypersonic inlet start/ unstart phenomena," *The Aeronautical Journal*, vol. 113, no. 1142, pp. 263–271, 2008.

[7] J. Chang, B. Li, W. Bao, W. Niu, and D. Yu, "Thrust control system design of ducted rockets," *Acta Astronautica*, vol. 69, no. 3, pp. 86–95, 2011.

[8] J. Chang, B. Li, W. Bao, W. Niu, and D. Yu, "Friction-compensation control of gas-flow regulation for ducted rockets based on adaptive dither method," *Journal of Aerospace Engineering*, vol. 26, no. 4, pp. 715–720, 2013.

[9] J. Ma, L. Qian, G. Chen, and M. Li, "Dynamic analysis of mechanical systems with planar revolute joints with clearance," *Mechanism and Machine Theory*, vol. 94, pp. 148–164, 2015.

[10] Q. Tian, P. Flores, and H. M. Lankarani, "A comprehensive survey of the analytical, numerical and experimental methodologies for dynamics of multibody mechanical systems with clearance or imperfect joints," *Mechanism and Machine Theory*, vol. 122, pp. 1–57, 2018.

[11] S. Z. Yan, W. W. Xiang, and T. Q. Huang, "Advances in modeling of clearance joints and dynamics of mechanical systems with clearances," *Acta Scientiarum Naturalium Universitatis Pekinensis*, vol. 52, no. 4, pp. 741–755, 2016.

[12] W. Xiang, S. Yan, J. Wu, and W. Niu, "Dynamic response and sensitivity analysis for mechanical systems with clearance joints and parameter uncertainties using Chebyshev polynomials method," *Mechanical Systems and Signal Processing*, vol. 138, p. 106596, 2020.

[13] A. Wang and Q. H. Zeng, "Load characteristics and modeling methods for the flow regulator of a solid ducted rocket," *International Journal of Aerospace Engineering*, vol. 2019, Article ID 8031290, 10 pages, 2019.

[14] N. Lei and W. Xiong, "Research on the deposition at the SDR by foreign scholars," *Journal of Propulsion Technology*, vol. 6, no. 2, pp. 89–94, 2019.

[15] B. Evans, K. K. Kuo, and A. C. Cortopassi, "Characterization of nozzle erosion behavior under rocket motor operating conditions," *International Journal of Energetic Materials and Chemical Propulsion*, vol. 9, no. 6, pp. 533–548, 2010.

[16] C. O. Alanyalioglu, "Simple and accurate method for determination of solid rocket motor nozzle throat history," in *53rd AIAA/SAE/ASEE Joint Propulsion Conference*, GA, USA, July 2017.

[17] Y. Li, Y. Zhou, Z. Sun, D. Sun, and L. Ma, "Discrimination technology for the nozzle throat diameter erosion performance of solid rocket motor," *Journal of Projectiles, Rockets, Missiles and Guidance*, vol. 40, no. 2, pp. 60–62, 2020.

[18] A. Alan, Y. Yildiz, and U. Poyraz, "Adaptive pressure control experiment: controller design and implementation," in *IEEE conference on control technology and applications*, Maui, HI, USA, August 2017.

[19] W. Y. Niu, W. Bao, J. Chang, T. Cui, and D. R. Yu, "Control system design and experiment of needle-type gas regulating system for ducted rocket," *Proceedings of the Institution of Mechanical Engineers, Part G: Journal of Aerospace Engineering*, vol. 224, no. 5, pp. 563–573, 2010.

[20] Y. X. Liu, *Study on control system of the throttleable ducted rocket, [Ph.D.'s thesis]*, Beijing Institute of Technology, Beijing, China, 2015.

[21] J. Lee, J. Kim, H. Jang, and J. Oh, "Experimental and theoretical investigations of thrust variation with pintle positions using cold gas," in *44th AIAA/ASME/SAE/ASEE Joint Propulsion Conference & Exhibit*, CT, USA, July 2008.

[22] H. Ko and J. Lee, "Cold tests and the dynamic characteristics of the pintle type solid rocket motor," in *49th AIAA/ASME/SAE/ASEE Joint Propulsion Conference*, CA, USA, July 2013.

[23] P. C. Pinto and G. Kurth, "Robust propulsion control in all flight stages of a throttleable ducted rocket," in *47th AIAA/ASME/SAE/ASEE Joint Propulsion Conference & Exhibit*, San Diego, California, 2011.

[24] A. Wang, Q. Zeng, L. Ma, and H. Wang, "Virtual free-volume revised method and adaptive control for solid ducted rockets," *Journal of Aerospace Engineering*, vol. 34, no. 5, p. 04021053, 2021.

[25] W. Y. Wang, B. Liu, and V. Kodur, "Effect of temperature on strength and elastic modulus of high-strength steel," *Journal of Materials in Civil Engineering*, vol. 25, no. 2, pp. 174–182, 2013.

[26] W. Li, H. Kou, X. Zhang et al., "Temperature-dependent elastic modulus model for metallic bulk materials," *Mechanics of Materials*, vol. 139, no. 9, p. 103194, 2019.

[27] X. Deng, J. Fu, and Y. Zhang, "A predictive model for temperature rise of spindle–bearing integrated system," *Journal of Manufacturing Science and Engineering*, vol. 137, no. 2, p. 021014, 2015.

[28] B. B. Chen, *Research on the combustion process and combustion technology of Boron-based solid ducted rockets, Ph.D.'s thesis*, National University of Defense Technology, Changsha, China, 2018.

[29] E. Elsaka, S. Elbasuney, H. E. Mostafa, T. Elhedery, and A. M. Eldakhakhny, "Burning rate measurement of composite propellant using acoustic wave emission in comparison with other techniques," *Journal of Engineering Science and Military Technologies*, vol. 4, no. 2, pp. 226–232, 2020.

[30] H. Yaman, V. Celik, and E. Degirmenci, "Experimental investigation of the factors affecting the burning rate of solid rocket propellants," *Fuel*, vol. 115, no. 6, pp. 794–803, 2014.